Geophys. J. Int. (2004) **157,** 865–870 doi: 10.1111/j.1365-246X.2004.02275.x

FAST TRACK PAPER

The signatures of tectonics and glacial isostatic adjustment revealed by the strain rate in Europe

Anna Maria Marotta and Roberto Sabadini

Geophysics Section, Department of Earth Sciences, University of Milan, L. Cicognara, 7 I-20129 *Milan, Italy. E-mail: anna.maria.marotta@unimi.it*

Accepted 2004 February 25. Received 2003 December 1; in original form 2003 July 2

SUMMARY

Tectonics and glacial isostatic adjustment (GIA) are simultaneously taken into account in order to quantitatively define their role in crustal deformation in Europe. A spherical finite-element model, based on the thin viscous shell approach and suitable for predicting tectonic deformation, and a spherical stratified viscoelastic Earth model, based on the normal mode approach to quantifying the effects of GIA, are used to predict intraplate deformation in Europe. Model predictions are compared with the geodetic strain rate obtained from ITRF2000 velocity solutions. Our results confirm that both geophysical processes influence intraplate deformation in Europe, with tectonics playing the leading role south of Potsdam and GIA being the only mechanism north of Onsala. Both geophysical processes affect the deformation at intermediate latitudes, where the contributions to the deformation coming from tectonics and GIA are of the same magnitude and the combined tectonic plus GIA model succeeds in reproducing the eigendirections of the local predominantly SSW–NNE directed compression. The stiffening in the East European Platform is crucial for shielding the northeastern regions from the compressional effects of Africa–Eurasia convergence and to allow SE–NW directed extension in Fennoscandia driven by GIA.

Key words: glacial isostatic adjustment, strain rate, tectonics.

1 INTRODUCTION

Africa–Eurasia convergence and GIA are major geophysical processes in Europe: their signatures can now be revealed by means of geodetic deformation patterns obtained from the ITRF2000 network covering the whole of Europe. Since ITRF2000 velocity solutions hold both tectonic and GIA information, a comparison between the strain rates from geophysical modelling and the geodetic observations from ITRF2000 permits us to discriminate among different tectonic hypotheses and, in particular, to reveal how plates interact in a wide region from northern Europe to the Mediterranean and from the Iberian Peninsula to the Aegean Sea and Anatolia. In recent years several authors have focused on the effects on intraplate deformation of GIA at high latitudes (e.g. Milne *et al.* 2001) and of tectonics in central and southern Europe (e.g. Golke & Coblentz 1996; Marotta et al. 2001) but solely speculative hypotheses about the concurrent role of both mechanisms on the strain field have been proposed. The published literature thus lacks any quantitative study in which the effects of both mechanisms are compared, to support the reliability of these hypotheses. This study aims to make a significant contribution in this direction, since for the first time crustal deformation in Europe is predicted by taking into account the cumulative effects of tectonics and GIA. A first attempt at this has already been made by Marotta & Sabadini (2002). However, that study had some limitations, such as a limited extension of the study domain which did not include Fennoscandia, where the effect of GIA is expected to be the largest; furthermore, it was a 1-D analysis since the predicted and the observed crustal deformation were compared along baselines connecting pairs of geodetic sites; finally, the two mechanisms were still analysed separately. The present study differs from this previous analysis in several aspects. First of all, it uses a 2-D approach within a wider region, by analysing the deformation within triangular regions bounded by the lines connecting three geodetic sites. The quantitative comparison of the predicted crustal deformation obtained by the combined tectonic plus GIA model and geodetic data will be discussed.

2 TECTONIC MODEL

We adopt an incompressible, viscous model to investigate tectonic deformation in Europe driven by Africa–Eurasia convergence and mid-Atlantic ridge opening (Fig. 1). The deformation field is computed using the numerical approach described in detail in Marotta *et al.* (2001), adapted to take into account the sphericity of the Earth. The lithosphere is modelled as a stratified viscous shell with a constant total thickness overlying an inviscid asthenosphere. The

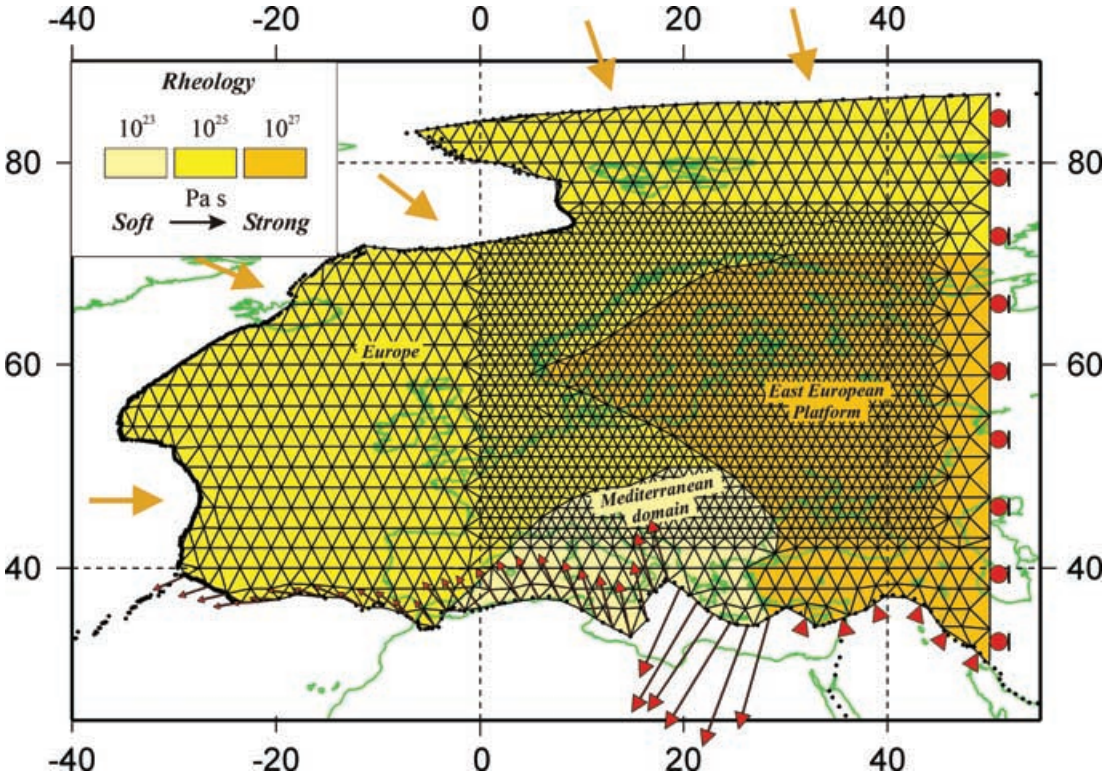

Figure 1. Finite-element grid and boundary conditions for the area under study. The grid distinguishes three major blocks, or subdomains: the European, East European Platform and Mediterranean. The thick yellow arrows at the left and top sides of the domain represent ridge push forces. The counter-clockwise rotation of the African Plate with respect to the European Plate, adopted from NUVEL-1A, and the geodetically determined velocities along the Aegean Trench McClusky *et al.* (2000) is reflected by the red arrows at bottom left. The southern border between the model domain and the Arabian region is held fixed (red triangles), while the right (eastern) boundary of the model is assumed to be shear stress free (red dots).

western and the northern borders of the model domain coincide with the location of the mid-Atlantic ridge, while the southern border coincides with the Africa–Eurasia plate contact. The eastern border of the model domain lies along the 45°E meridian, inside the intracratonic East European Platform, where the level of stress from the applied boundary velocity is expected to be small. The domain is discretized using planar triangular elements which are sufficiently small in size ($2^\circ \times 2^\circ$ being the maximum extension in the western oceanic portion of the domain) to justify treating the surface of each individual grid element as flat. The governing equations (eqs (2) in Marotta *et al.* 2001), take the following form in spherical coordinates and a stationary regime:

$$\frac{\partial}{\partial\theta}\left[2\bar{\mu}\left(\frac{\partial u_\theta}{\partial\theta}+u_{\rm r}\right)\right]+\frac{1}{\sin\theta}\frac{\partial}{\partial\phi}\left[\bar{\mu}\left(\frac{1}{\sin\theta}\frac{\partial u_\theta}{\partial\phi}+\frac{\partial u_\phi}{\partial\theta}-u_\phi\cot g\theta\right)\right]+\left[2\bar{\mu}\left(\frac{\partial u_\theta}{\partial\theta}-\frac{1}{\sin\theta}\frac{\partial u_\phi}{\partial\phi}-u_\theta\cot g\theta\right)\right]\cot g\theta = \frac{g\rho_{\rm c}R}{2L}\left(1-\frac{\rho_{\rm c}}{\rho_{\rm m}}\right)\frac{\partial S^2}{\partial\theta} \quad (1)$$

$$\frac{\partial}{\partial\theta}\left[\bar{\mu}\left(\frac{1}{\sin\theta}\frac{\partial u_\theta}{\partial\phi}+\frac{\partial u_\phi}{\partial\theta}-u_\phi\cot g\theta\right)\right]+\frac{1}{\sin\theta}\frac{\partial}{\partial\phi}\left[2\bar{\mu}\left(\frac{1}{\sin\theta}\frac{\partial u_\phi}{\partial\phi}+u_\theta\cot g\theta+u_{\rm r}\right)\right]+\left[2\bar{\mu}\left(\frac{\partial u_\phi}{\partial\theta}+\frac{1}{\sin\theta}\frac{\partial u_\theta}{\partial\phi}-u_\phi\cot g\theta\right)\right]\cot g\theta = \frac{g\rho_{\rm c}R}{2L}\left(1-\frac{\rho_{\rm c}}{\rho_{\rm m}}\right)\frac{1}{\sin\theta}\frac{\partial S^2}{\partial\phi} \quad (2)$$

where u_θ and u_ϕ are the components of the velocity along the co-latitude θ and longitude ϕ, respectively. $\bar{\mu}$ denotes the vertically averaged viscosity of the lithosphere, S and L are the crustal and lithosphere thickness respectively while $\rho_{\rm c}$ and $\rho_{\rm m}$ denote their uniform densities of 2800 and 3200 kg m^{-3}, respectively. g denotes the acceleration due to gravity while R represents the mean Earth radius. The radial velocity $u_{\rm r}$ is eliminated from these equations by invoking incompressibility and by assuming that the radial strain rate $\partial u_{\rm r}/\partial r$ vanishes. Under these assumptions, $u_{\rm r}$ can be expressed as

$$u_{\rm r} = -\frac{1}{2}\left(\frac{\partial u_\theta}{\partial\theta}+\frac{1}{\sin\theta}\frac{\partial u_\phi}{\partial\phi}+u_\theta\cot g\theta\right). \quad (3)$$

Thus, the thin shell model is a reliable predictor of the horizontal components of the velocity field u_θ, u_ϕ only. The major forces acting on the system are the horizontal tectonic push from Africa–Eurasia convergence and mid-Atlantic spreading, and the horizontal stresses controlled by the horizontal variations in crustal thickness. As a consequence of the latter assumption, the model is a reliable predictor of horizontal components of strain rate only. Once the crustal thickness S and the boundary conditions are specified, the numerical integration of eqs (1) and (2) yields the stationary 2-D tectonic velocity field. A distinct viscosity can be applied to each element of the model grid and this permits incorporation of lateral variations in lithospheric strength. With respect to this aspect, we consider three types of tectonic model in which the European lithosphere is treated as the reference domain where a viscosity of 10^{25} Pa s is prescribed (Fig. 1). In the Mediterranean domain, extending from the Tyrrhenian Sea to the eastern limit of the Pannonian Basin

Table 1. Tectonic models considered in the analysis.

Model	Rheological heterogeneities	Ridge boundary conditions (mm yr^{-1})
1	No rheological heterogeneities	5.0
2	No rheological heterogeneities	0.0
3	Stiff East European Platform	5.0
4	Stiff East European Platform	0.0

through the Adriatic Plate, the viscosity has been reduced by one order of magnitude with respect to the reference viscosity, to simulate the softening of the basin. The viscosity of the East European Platform, which encompasses most of the Caledonian Deformation Front, is increased by two orders of magnitude to reproduce the stiff Baltic Shield. The velocity boundary conditions are considered as fixed relative to the Eurasia Plate: the Africa–Eurasia continental convergence of the order of 1 cm yr^{-1} (southern boundary of the model domain to about 20°N) is prescribed by NUVEL-1A (red arrows, Fig. 1). With respect to a fixed Eurasia, we must consider the ridge push forces along the North Atlantic Ridge. In our simulations, the ridge push forces are parametrized in terms of velocity boundary conditions applied along the ridge (thick yellow arrows), thus simulating the line forces acting along the plate boundary, as shown in Richardson *et al.* (1979), ranging from 10^{12} N m^{-1} for a velocity of about 1 mm yr^{-1}, to 10^{13} N m^{-1} for 5 mm yr^{-1}, this last value representing an upper bound for ridge push forces (Richardson & Reding 1991). These velocities, which are used to parametrize the ridge push forces, are not constant along the ridge but are scaled with respect to the spreading rates deduced from NUVEL-1A. Along the Aegean Trench the velocity boundary conditions are obtained from McClusky *et al.* (2000) and reflect trench subduction forces. The eastern boundary of the model domain is fixed, in agreement with the hypothesis that we are considering Eurasia as fixed; since we are not interested in the deformation occurring east of the considered ITRF2000 network, we assume that east of longitude 50° the study domain is closed; in order to avoid too large an effect from artificial stress accumulation due to the closed eastern boundary we have imposed a condition of freedom from shear stress, as indicated by the red dots along the right boundary of the model. The conditions along our eastern boundary account for a possible decoupling between the western and eastern parts of the Eurasia Plate (Molnar *et al.* 1973) and imply that we are assuming that all the intraplate deformation of Eurasia due to Africa–Eurasia convergence and Atlantic Ridge push takes place within the studied domain. The contact between the East European Platform and the Arabian Plate is held fixed, as indicated by the red triangles in the southeast part of Fig. 1. NUVEL-1A indicates a northward-directed velocity on this boundary. However, as discussed by Jimenez-Munt & Sabadini (2002), the local stiffness of the lithosphere and the existence of a transcurrent fault at the northern boundary of the Arabian Plate produce little long-wavelength deformation to the north, where the ITRF2000 sites are located. The variation in crustal thickness used in the analysis has been obtained by linear interpolation onto the adopted grid of the model CRUST 2.0 (Bassin *et al.* 2000; http://mahi.ucsd.edu/Gabi/rem.html). Table 1 summarizes the characteristics of the tectonic models.

3 RESULTS AND DISCUSSION

In this section we discuss the results of our analysis in terms of strain-rate eigenvalues and eigendirections, computed for a set of triangular domains covering the study area and compared with the corresponding ones obtained from the ITRF2000 velocity solutions. Particular care is devoted to defining the final set of triangular domains where the analysis is applied. Although several criteria could be followed for choosing the triangulation, we adopt a combination of geometric and reliability criteria. We first select the subset of sites uniformly distributed through the study area in which the velocity is known with the lowest variance, and then we adopt the triangulation which is most representative of homogeneous tectonic units. Within each triangular domain the strain-rate eigenvalues $\dot{\epsilon}_1$ and $\dot{\epsilon}_2$ with the azimuth for the component $\dot{\epsilon}_2$, both for data and model predictions, are computed following the procedure described in Devoti *et al.* (2002). Table 2 lists the values of strain-rate eigenvalues and of the azimuth, with the corresponding errors, computed for ITRF2000 velocity solutions. The ITRF2000 solutions indicate a general pattern of SE–NW directed extension and SW–NE directed compression, both at low and high latitude. However, in the Fennoscandia region the ratio between extension and compression is significantly higher then in Central Europe. Another feature that is worth highlighting is the large uncertainties in strain-rate predictions at high latitudes, both in magnitude and in direction, making the SW–NE compression meaningless. Since the tectonic and GIA models, taken separately, show the tendency to underestimate the observed strain rates, direct comparison between data and prediction is carried out only in Fig. 5 (see later), where the combined effects of the best performing tectonic and GIA models are considered.

Fig. 2 shows the results of tectonic models 1 and 2. Except for POTS–PENC–BOGO and POTS–GRAZ–PENC where extension dominates (cyan bars), model 1 predicts SE–NW compression (yellow bars) due to the combined effects of Africa–Eurasia convergence and Atlantic Ridge spreading. The dominant extension in the triangle POTS–GRAZ–PENC has already been noted along the baseline POTS–PENC in Marotta & Sabadini (2002), where it has been attributed to the lateral extrusion induced by the Alpine Front. The striking result of model 1 is that the modelled compression is at right angles with respect to the observed one. The two triangles quoted above are the only ones in which we obtain complete agreement, in terms of extensional eigendirections and eigenvalues, between modelling results and observations. Another major problem with model 1 is that north of VIS0 the ITRF2000 data indicate extension, while the model predicts a dominant compression. This inconsistency suggests that the effects of ridge push are too large and this reduction could reduce the misfit. This hypothesis has been tested by considering the end-member model 2, in which no ridge push is considered. This extreme case implicitly assumes that the deformation due to ridge push takes place in that part of the domain between the ridge and the study area. As expected, in model 2 the previous disagreement between data and prediction is significantly reduced, with compression becoming negligible at high latitudes (red bars) and subject to a clockwise rotation in central Europe. The introduction of rheological heterogeneities in the tectonic model is crucial in our search for the best fit model (Fig. 3). When a velocity boundary condition of 5.0 mm yr^{-1} is prescribed along the Atlantic Ridge, we note a substantial modification in the strain-rate patterns north of the line connecting DELF to BOGO, where compression is reduced with respect to Fig. 2 (yellow bars) and SSW–NNE extension appears. The reduction of compression in the stiff Baltic Shield and south of it is easily understood in terms of the reduced flow within the high-viscosity region, which acts as a barrier that annihilates the propagation of the velocity driven by Africa–Eurasia convergence and Atlantic Ridge push within the Baltic Shield. When zero-velocity boundary conditions are assumed along the western boundary (model 4), the ridge push effects disappear everywhere,

Table 2. Observed strain rates as deduced from ITRF2000 GPS data.

Triangle	Eigenvalue $\dot{\epsilon}_1$ (nanostrain yr^{-1})	Eigenvalue $\dot{\epsilon}_2$ (nanostrain yr^{-1})	Azimuth of $\dot{\epsilon}_2$ (deg)
TOUL–ZIMM–DELF	$+3.20 \pm 1.38$	-2.66 ± 1.46	$+56.22 \pm 9.40$
MADR–TOUL–BRST	$+7.55 \pm 0.52$	-1.50 ± 1.43	$+11.80 \pm 4.53$
POTS–DELF–ZIMM	$+7.76 \pm 0.77$	-0.17 ± 0.89	$+26.49 \pm 5.69$
POTS–ZIMM–GRAZ	-0.29 ± 0.96	-3.00 ± 2.83	-44.26 ± 32.70
POTS–GRAZ–PENC	$+4.19 \pm 1.48$	-2.49 ± 2.21	$+27.91 \pm 8.53$
POTS–PENC–BOGO	$+4.42 \pm 3.83$	-2.48 ± 2.01	$+28.30 \pm 17.55$
POTS–BOGO–VIS0	$+5.77 \pm 2.07$	-4.96 ± 5.87	$+32.49 \pm 16.58$
POTS–VIS0–ONSA	$+5.26 \pm 1.54$	-0.25 ± 2.42	$+35.85 \pm 12.95$
POTS–ONSA–DELF	$+3.91 \pm 1.87$	-1.36 ± 1.49	$+19.31 \pm 14.96$
VIS0–BOGO–RIGA	$+6.43 \pm 2.91$	-1.69 ± 2.62	$+14.82 \pm 25.53$
TOUL–DELF–BRST	$+3.98 \pm 1.90$	-2.48 ± 3.80	$+25.12 \pm 19.47$
VIS0–RIGA–VAAS	$+10.26 \pm 0.79$	$+0.19 \pm 0.62$	$+19.02 \pm 3.52$
RIGA–JOEN–VAAS	$+6.62 \pm 2.51$	$+0.68 \pm 2.75$	$+20.75 \pm 20.21$
VAAS–JOEN–SODA	$+5.25 \pm 3.00$	-1.62 ± 2.28	$+18.12 \pm 16.69$
VAAS–TROM–VIL0	$+6.58 \pm 5.79$	-0.22 ± 1.63	$+33.99 \pm 25.91$
VAAS–SODA–TROM	$+8.34 \pm 6.03$	-1.61 ± 1.96	$+41.64 \pm 17.69$
ONSA–VIS0–VIL0	$+9.98 \pm 0.86$	-0.71 ± 0.83	$+25.63 \pm 3.11$
VIS0–VAAS–VIL0	$+9.41 \pm 0.84$	-2.30 ± 0.89	$+30.85 \pm 2.48$

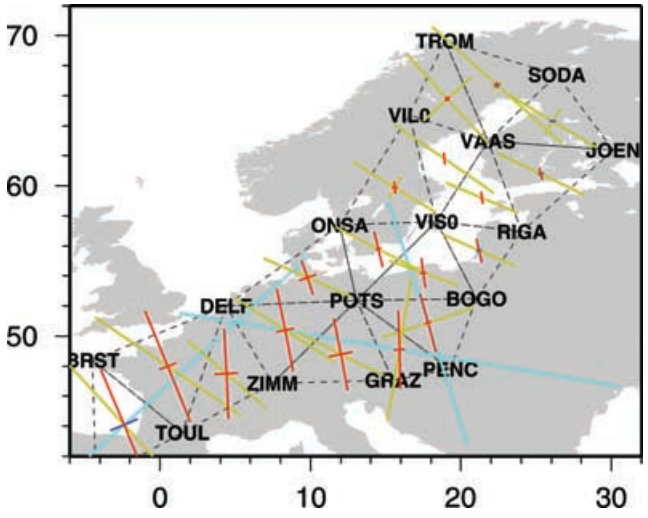

Figure 2. Directions of the strain-rate eigenvectors predicted by tectonic models 1 (cyan extension; yellow compression) and 2 (blue extension; red compression).

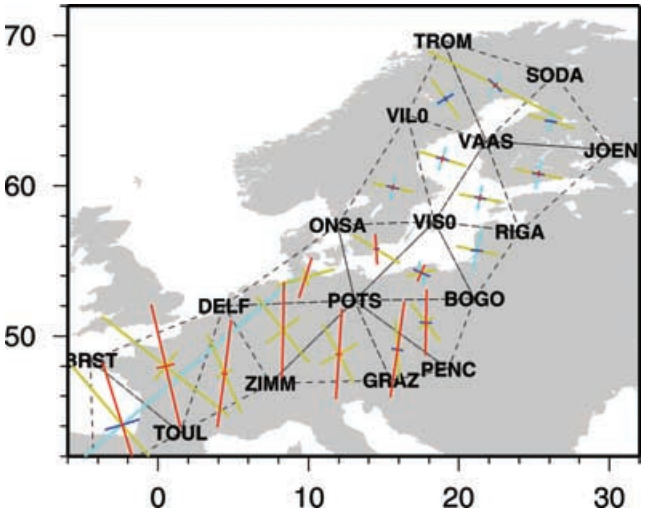

Figure 3. Directions of the strain-rate eigenvectors predicted by tectonic models 3 (cyan extension; yellow compression) and 4 (blue extension; red compression).

leaving space for the Africa indenter and to an increase in compression with respect to Fig. 2 (red bars). A significant rotation of the compressive eigendirections from NNW to NNE occurs south of Potsdam, in agreement with ITRF2000 data. Due to the stiffening of the Baltic Shield, the compressive effects of Africa–Eurasia push almost disappear north of VIS0, supporting the hypothesis that another geophysical process must be invoked to explain the large SE–NW extension. Previous works (Milne *et al.* 2001; Marotta & Sabadini 2002) have shown that GIA is the dominant mechanism in Fennoscandia. In the following figures, the impact of GIA is shown on the strain-rate tensor rather than on the velocity field at geodetic sites or baselines connecting pairs of sites, as in Milne *et al.* (2001), Marotta & Sabadini (2002). The GIA models are the same as in Marotta & Sabadini (2002). Models shown in Fig. 4 are characterized by an upper mantle viscosity of 0.5×10^{21} Pa s and a lower mantle viscosity of 10^{21} Pa s (blue and red bars), GIA21, or 10^{22} Pa s (cyan and yellow bars), GIA22. A 120 km thick lithosphere of 10^{25} Pa s is considered, as in the tectonic model. GIA21 predicts SE–NW extension in Fennoscandia (blue bars), in agreement with the geodetic data, and negligible SE–NW compression in the south (red bars). A peculiar situation is visible south of VIS0 and north of POTS, where GIA21 predicts a SSE–NNW compression comparable in magnitude to that induced by the tectonic model characterized by the stiff Baltic Shield, with no ridge push: Figs 3 and 4 thus suggest that both tectonics and GIA contribute to the compression in the range of latitudes of 52° and 58°, in the region between Fennoscandia and central continental Europe. We should note, however, that extension in Fennoscandia is generally underestimated by GIA21. The extension in the north and the small compression at latitudes between 52° and 58° are due to the outward motion from the centre of deglaciation and small northerly oriented velocities due to GIA in continental Europe, as visible in the velocity pattern for the uniform viscosity model in Fig. 3 of Marotta & Sabadini (2002). An increase in the extension north of

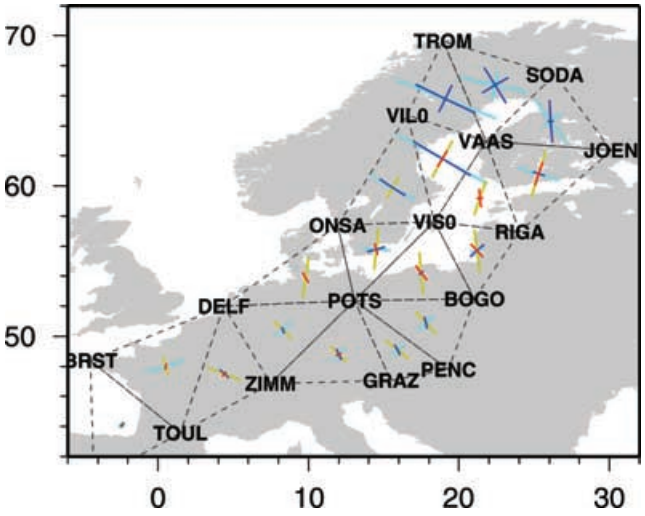

Figure 4. Directions of the strain-rate eigenvectors (bars) predicted by GIA models (blue extension and red compression refer to an upper mantle viscosity of 0.5×10^{21} Pa s and a lower mantle viscosity of 10^{21} Pa s (GIA21); cyan extension and yellow compression refer to an upper mantle viscosity of 0.5×10^{21} Pa s and a lower mantle viscosity of 10^{22} Pa s (GIA22)).

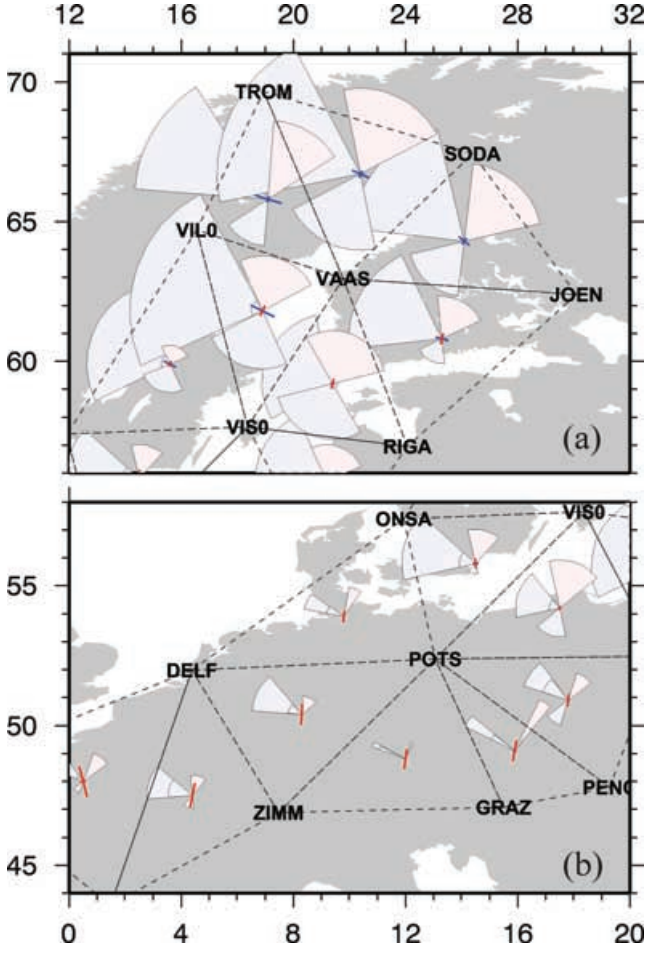

Figure 5. Strain-rate eigenvalues and eigenvectors (bars) predicted by the combination of the tectonic model 3 plus GIA22 (a) and by the tectonic model 3 plus GIA21 (b) (blue extension; red compression), compared with observed strain rates, based on ITRF2000 velocity solutions (Table 2) (light blue and light red circular sectors for extension compression, respectively).

latitude 60° is obtained by means of GIA22. The extension is now increased in all the triangles (cyan bars), and, north of VIS0, the fit with the geodetic strain rate is improved, within the uncertainties. South of the line connecting ONSA and VIS0, and north of POTS, we note that compression (yellow bars) is increased with respect to GIA21. South of POTS, the contribution of this GIA model to both compression and extension is no longer negligible, as for GIA21, but compression points in the SE–NW direction, in contrast with observation. When comparison of Fig. 4 is made with Fig. 3, we note that the tectonic model with the stiff Baltic Shield influences the compression south of ONSA–VIS0, with largest contributions south of DELF–POTS–BOGO, while GIA contributes to the compression in the central European region between ONSA–VIS0 and DELF–POTS–BOGO and to the extension north of ONSA–VIS0: these figures thus confirm that tectonics dominates the strain-rate pattern south of POTS, while GIA is the dominant mechanism north of VIS0 in Fennoscandia and that both tectonics and GIA contribute to the deformation in the European continental region between the latitudes of POTS and VIS0. That this is the case is shown in Fig. 5 in which the combined effects of the best performing tectonic model 3 and GIA models are portrayed, with Figs 5(a) and (b) referring to the northern and southern domains. Model predictions denoted by the bars are superimposed to the strain rates of Table 2, represented with their errors in the magnitude and azimuth, with light blue denoting extension and light red compression. It should be noted that the data are portrayed for only one side of the admissible area of variability of the magnitude: this leaves room for depicting the already highlighted possible change from compression into extension, or vice versa, caused by some errors being larger in absolute value than the corresponding datum. Model results reproduce well the general pattern of NW extension in Fig. 5(a), while in Fig. 5(b) only the NE compression is reproduced. It should also be noted that the agreement in the azimuth is obtained by combining the tectonic model 3 with GIA22 for high latitudes (Fig. 5a) and with GIA21 for intermediate latitudes (Fig. 5b), which may support the existence of lateral variations in mantle viscosity with a stiffer mantle underneath the Baltic Shield, coherently with the lateral heterogeneities built in the tectonic model not accounted for in the GIA models.

As far as the amplitude is concerned, model predictions have the tendency to reproduce the lower bounds of the observed strain rates, in particular for high latitudes, which may be due to several reasons. For high latitudes it could be due to the usage of a viscosity profile derived from time-dependent gravity studies (Sabadini *et al.* 2002) or to the incompressibility of the model. For intermediate latitudes (Fig. 5b) a possible cause could be our use of NUVEL-1A, model that although being the necessary reference for our tectonic modelling turns out to be inadequate, to the level of a few millimetres per year, to describe the current relative plate motion (Altamini *et al.* 2002). We have verified, in fact, that a 50 per cent increase in the relative Eurasia–Africa convergence produces an increase of approximately the same amount in the predicted compressive strain rates in Fig. 5(b).

4 CONCLUSIONS

We have analysed the combined effects induced by tectonics and GIA on the deformation in continental Europe. Our results indicate that Africa–Eurasia convergence plays the dominant role in the part of Europe extending from the Alps up to about latitude 52°N, corresponding to the latitude of Potsdam (POTS); this tectonic mechanism has no effect north of about latitude58°N, corresponding to

the latitude of Onsala (ONSA), in Fennoscandia. GIA is the only mechanism which has a signature north of Onsala. The strain rate in central Europe, between Onsala and Potsdam, is clearly affected by both mechanisms. Our analysis thus reinforces the conclusions of previous studies based on baseline rate of changes (Marotta & Sabadini 2002; Marotta *et al.* 2004), that deformation in Europe is the result of a complex interplay between forces induced by tectonics and GIA. Lateral variations in lithospheric strength in the East European Platform play a crucial role in separating the two domains where tectonics and GIA have their major influence, south of Potsdam and north of Onsala respectively. The combination of the tectonic model, characterized by a stiff East European Platform and Atlantic Ridge push effects completely absorbed within the western oceanic portion of the model domain, and the GIA models turns out to be the best performing one, once its predictions are compared with geodetic strain rates. This best performing model reproduces the observed compression south of Onsala and the dominant SE–NW extension north of Onsala.

ACKNOWLEDGMENTS

This work was funded by the Italian Ministry of Universities and Research (M.I.U.R.) under the project 'A multidisciplinary monitoring and multiscale study of the active deformation in the northern sector of the Adria Plate' (COFIN 2002). All figures were created using the GMT plotting software (Wessel & Smith 2001). The authors thank Bruno Crippa for support during the data processing and the reviewers Bert Vermeersen and Detlef Wolf for their comments and suggestions.

REFERENCES

Altamini, Z., Sillard, P. & Boucher, C., 2002. ITRF2000: a new release of the International Terrestrial Reference Frame for Earth science applications, *J. geophys. Res.,* **107,** 2001JB000561.

Bassin, C., Laske, G. & Masters, G., 2000. The current limits of resolution for surface wave tomography in North America, *EOS, Trans. Am. geophys. Un.,* **81,** 897.

Devoti, R. *et al.*, 2002. Geophysical interpretation of geodetic deformation in the central Mediterranean area, *Tectonophysics,* **246,** 151–167.

Golke, M. & Coblentz, D., 1996. Origins of the European regional stress field, *Tectonophysics,* **266,** 11–24.

ITRF2000 *http://lareg.ensg.ign.fr/ITRF/ITRF2000*

Jimenez-Munt, I. & Sabadini, R., 2002. The block-like behavior of Anatolia envisaged in the modelled and geodetic strain, *Geophys. Res. Lett.,* **29,** 39/1–39/4.

Marotta, A.M. & Sabadini, R., 2002. Tectonic versus glacial deformation in Europe, *Geophys. Res. Lett.,* **29,** 73/1–73/4.

Marotta, A.M., Bayer, U., Scheck, M. & Thybo, H., 2001. The stress field below the NE German basin: effects induced by the Alpine collision, *Geophys. J. Int.,* **144,** F8–F12.

Marotta, A.M., Mitrovica, J.X., Sabadini, R. & Milne, G., 2004. Combined effects of tectonics and glacial isostatic adjustment on intra-plate deformation in central and northern Europe: applications to geodetic baseline analysis, *J. geophys. Res.* **109,** 2002JB002337.

McClusky, S. *et al.*, 2000. Global Positioning System constraints on plate kinematics and dynamics in the eastern Mediterranean and Causasus, *J. geophys. Res.,* **105,** 5695–5719.

Milne, G.A., Davis, J.L., Mitrovica, J., Scherneck, H.G., Johansson, J.M., Vermeer, M. & Kouvula, H., 2001. Space geodetic constrains on glacial isostatic adjustment in Fennoscandia, *Science,* **291,** 2381–2385.

Molnar, P., Fitch, T.J. & Wu, F.T., 1973. Fault plane solutions of shallow earthquakes and contemporary tectonics in Asia, *Earth planet. Sci. Lett.,* **19,** 101–112.

Richardson, R.M. & Reding, L., 1991. North American plate dynamics, *J. geophys Res.,* **96,** 12 201–12 223.

Richardson, R.M., Solomon, S.C. & Sleep, N.H., 1979. Tectonic stress in the plates, *Rev. Geophys.,* **17,** 981–1019.

Sabadini, R., Di Donato, G., Vermeersen, L.L.A., Devoti, R., Luceri, V. & Bianco, G., 2002. Ice mass loss in Antarctica and stiff lower mantle viscosity inferred from the long wavelength time dependent gravity field, *Geophys. Res. Lett.,* **29,** 11/1–11/4.

Wessel, P. & Smith, W.M.F., 2001. New improved version of Generic Mapping Tools released, *EOS, Trans. Am. geophys. Un.,* **79,** 579.